RSC Advances

Sensing properties of pristine, Al-doped, and defected boron nitride nanosheet toward mercaptans: A first-principles study

Journal:	*RSC Advances*
Manuscript ID	RA-ART-05-2015-009923.R3
Article Type:	Paper
Date Submitted by the Author:	11-Oct-2015
Complete List of Authors:	Heidari, Hassan; Azarbaijan Shahid Madani University, Chemistry Afshari, Sadegh; Azarbaijan Shahid Madani University, Chemistry Habibi, Esmaeil; Urmia University,
Subject area & keyword:	Nanomaterials - Nanoscience < Nanoscience

Sensing properties of pristine, Al-doped, and defected boron nitride nanosheet toward mercaptans: A first-principles study

Hassan Heidari[a*], Sadegh Afshari [a,b*], Esmaeil Habibi[c]

[a]*Department of Chemistry, Azarbaijan Shahid Madani University, P. O. Box: 53714-161, Tabriz, Iran*

[b]*Young Researchers and Elite club, Tabriz Branch, Islamic Azad University, Tabriz, Iran*

[c]*Nanotechnology Research Center, University of Urmia, Urmia, Iran*

[*] Corresponding authors. Fax: +98 412 432 7541; E-mail addresses: hassan_heidari@ymail.com, hassan_heidari@azaruniv.edu (H. Heidari)
sadegh.afshari@gmail.com (S. Afshari)

Abstract

The adsorption of mercaptans on the pristine, Al-doped, and mono-vacancy and Stone–Wales defected hexagonal boron nitride (h-BN) nanosheets was studied by density functional theory method at the wB97X-D/6-311G(d) level of theory. Two types of mercaptans (i.e., methyl and ethyl mercaptan) were chosen as the adsorbates. No adsorption was observed on the pristine and defected h-BN nanosheet except for B-vacancy defected h-BN nanosheet which the adsorption was exothermic. In the case of the Al-doped h-BN nanosheet with substituted boron and nitrogen defect site not only the adsorption was observed for both methyl and ethyl mercaptan but also their adsorption were exothermic. It was suggested that Al-doped h-BN nanosheet and B-vacancy defected h-BN nanosheet be a potential resource for adsorbing mercaptans. The electronic properties of all kinds of the studied h-BN nanosheets and adsorption configuration of mercaptans on them were reported.

Keywords: Boron nitride nanosheet, Al doping, Density functional theory, Mercaptans, Electronic properties

1. Introduction

Reduced sulfur compounds (RSCs) have a great impact on global atmospheric chemistry and play a significant role in the formation of atmospheric aerosols and, eventually, in the processes of global climate change [1]. Mercaptans or thiol compounds are included in the RSCs. They are introduced into the atmosphere by natural (originated from the reduction of sulfate existing in aerobic waters and soils) and anthropogenic sources (originated from fossil fuel burning, petrochemical industry or municipal sewage systems) [2-4].. Hence, development of an efficient monitoring method to detect such contaminants is an important topic for environmental protection.

Boron nitride (BN) is a chemical compound which is isoelectronic and isostructural with carbon [5]. BN mainly contains four types of isomers which are respectively: hexagonal boron nitride (h-BN), trigonal boron nitride (r-BN), cubic boron nitride (c-BN), and wurtzite boron nitride (w-BN) [6, 7]. h-BN is an interesting substance, which can be synthesized in various forms including nanosheets, nanotubes, and nanohorns like graphitic materials [8] and h-BN has attracted considerable attentions due to its wide HOMO-LUMO gap semiconducting property, high melting point, low density, high mechanical strength, oxidation resistance, outstanding thermal, and electrical properties [9-13]. Similar to its other morphology, such as nanotube, the pristine h-BN nanosheet is intrinsically insulators or wide HOMO-LUMO gap semiconductors, which is not ideal for electronic applications and is almost inert to many gas molecules [14-16]. Therefore, it is very important to overcome this obstacle and increase sensitivity of the BN toward some important gas molecules in aspects of environmental and medical monitoring. Sensitivity of the BN can be widened and enhanced substantially through doping technology or defect [17-22]. Neetu et al. [23] established that substitutional C doping of the boron nitride nanotubes (BNNT) is an effective method for removal and detection of a HF molecule. Moradi et al. [21] showed that

interaction of mono vacancy defected h-BN with the NO molecule is energetically more favorable than pristine and Stone–Wales (SW) defected nanosheet. Noorizadeh et al. [22] found that formaldehyde can be chemically adsorbed on Al-doped and N-vacancy defected h-BN sheets with appreciable adsorption energies. Anota et al.[18] studied adsorption of monomer of chitosan on h-BN nanosheet and the results indicate that the interactions between the monomer of chitosan and the h-BN nanosheet yield chemisorptions. On the other hand N-N and B-N di-vacancies improved the chemical adsorption of the monomer on the nanosheet surface. Beheshtian et al.[24] found that the phosgene molecule interacts with the pristine boron nitride nanotubes (BNNT) via van der Waals forces, but it presents much higher reactivity toward the Sc-doped BNNT.

In this study we explored, for the first time, the adsorption of methyl mercaptan (MeSH) and ethyl mercaptan (EtSH), as significant pollutants, on the pristine, Al doped, and mono-vacancy and SW defected h-BN nanosheets by density functional theory (DFT) calculations. We report that the sensitivity of h-BN nanosheet to mercaptans gases could be enhanced to a higher level based on DFT calculations through B-vacancy defect and Al doping.

2. Computational methods

All calculations were performed using DFT at wB97X-D/6-311G(d) level of theory as implemented in the GAMESS suite of program [25]. The wB97X-D is the latest functional developed by Head-Gordon and Chai that yields satisfactory accuracy for thermochemistry, kinetics, and non-covalent interactions [26]. Density of states (DOS) for structures has been obtained by GaussSum program [27]. In graphs of DOS, E_g generally refers to the energy difference between the valence (HOMO) and the conduction levels (LUMO) in semiconductors.

For the sake of clarity, the Fermi level has been set to zero. In order to verify the structures, corresponding frequency calculations were carried out at the same level. The adsorption energy (E_{ad}) of a molecule adsorbed on a nanosheet is obtained using the following equation:

$$E_{ad} = E(_{molecule + nanosheet}) - E_{molecule} - E_{nanosheet} \quad (1)$$

where $E(_{molecule + nanosheet})$ is the total energy of a MeSH or EtSH molecule adsorbed on the nanosheet, $E_{molecule}$ is the energy of the isolated MeSH or EtSH molecule, and $E_{nanosheet}$ is the energy of the isolated nanosheet. Here pristine, some defected types, and Al-doped h-BN nanosheet were used as nanosheet. Chigo and coworker [28] showed that the HOMO-LUMO gap for clusters with 19 hexagons differs by only 10^{-2} eV/atom from the corresponding value for bigger clusters (37 and 70 hexagons). Therefore, the h-BN nanosheet consisting 28 hexagons (39B and 39N atoms) was considered and the end atoms were saturated by hydrogen atoms (24H atoms). The negative and positive values of E_{ad} indicate the exothermic or endothermic process of the adsorption, respectively. The net charge transfer (Q_T) from the MeSH or EtSH molecule to the Al_N-doped, Al_B-doped, and B-vacancy defected h-BN nanosheets is calculated by using Mulliken population analysis, which is defined as the charge difference between the MeSH or MeSH molecule adsorbed on the nanosheet and an isolated MeSH or EtSH molecule.

3. Results and discussion

3.1. Adsorption of mercaptans on pristine h-BN nanosheet

In the first step, we started by performing the geometry optimization of h-BN nanosheet and mercaptans molecules. For h-BN nanosheet this was accomplished by considering a BN nanosheet consisting 28 hexagons. Optimized geometries of h-BN nanosheet, MeSH and EtSH are presented in Fig. 1. A B–N length of approximately 1.448 Å was obtained for the pristine h-

BN nanosheet, in accordance with previous theoretical results[19, 21]. The free MeSH and EtSH molecules achieved with a C–S bond length of 1.821 and 1.828 Å for MeSH and EtSH, respectively. Then, we search the best adsorption geometry of MeSH and EtSH on pristine h-BN nanosheet and hence, various possible adsorbing configurations are investigated. MeSH and EtSH molecules were initially placed above a B or N atom or the center of the ring, with the MeSH and EtSH molecules oriented perpendicular (with the C or S atom pointing towards the h-BN nanosheet) to the h-BN nanosheet. Several other configurations with the MeSH and EtSH molecules placed parallel to the h-BN nanosheet were also tested. After full relaxation, no distinct structural change has been found. It is also found that in all configurations distances between the mercaptans molecules and h-BN nanosheet are too long, about 4 Å, and this show that mercaptans molecules do not undergo physisorption or chemisorption on pristine h-BN nanosheet. This indicates that the pristine h-BN nanosheet is insensitive to mercaptans molecules.

3.2. Adsorption of mercaptans on mono-vacancy and Stone–Wales defected h-BN nanosheet

As no interaction between mercaptans and pristine h-BN nanosheet was observed, therefore, in this section, our intention is to verify whether or not a vacancy-type defect can improve the adsorption phenomena. Fig. 1 shows optimized geometries of N-vacancy and SW defected h-BN nanosheets. As can be seen, N-vacancy defect induce a reconstructed structure, which consists of a pentagonal ring. SW defected h-BN nanosheet also consists of two pairs of five-membered and seven-membered rings. But, B-vacancy not leads to the formation of a pentagonal structure (Fig. 2a). Similar to pristine h-BN nanosheet, we explore various possible adsorbing configurations of the mercaptans molecules on the defected h-BN nanosheet. The results indicated that no

adsorption of mercaptans molecules on defected h-BN nanosheets in all of its configurations is observed except for B-vacancy defected h-BN nanosheet. In B-vacancy defected h-BN nanosheet when MeSH or EtSH was placed perpendicular with S atom pointing towards the center of the defected ring an adsorption between S atom and N atom were observed and its corresponding calculated E_{ad} values are -43.10 and -44.78 kcal mol^{-1} for MeSH and EtSH, respectively, indicating that adsorption is exothermic (Fig. 2). After adsorption the mean S-N bond length was 1.820 and 1.822 Å for MeSH and EtSH, respectively. The adsorption of MeSH or EtSH molecule affects on the B-vacancy defected h-BN nanosheet by inducing a small bending of the nanosheet. The large E_{ad} values of MeSH and EtSH on B-vacancy defected h-BN nanosheet reveals the chemical nature of the interaction. Mulliken charge analyses were also performed to evaluate the amount of electron transfer between the studied nanosheets and mercaptans molecules. The amounts of Q_T are given in Table 1. The high amount of the charge transfer (Table 1) between mercaptans molecules and B-vacancy defected h-BN nanosheet proves the nature of the interaction. Polarities are also obtained in the most stable geometries and are given in Table 1. The numerical values showed that the adsorption of mercaptans molecules on B-vacancy defected h-BN nanosheet cause an increase in value of polarities in comparison with unadsorbed form.

3.3. Adsorption of mercaptans on Al-doped h-BN nanosheet

In this section we studied the effect of doping of Al atoms in h-BN nanosheet toward mercaptans molecules. The geometric structures are first optimized for Al at B or N site doped h-BN nanosheet (denoted by Al_B or Al_N, respectively) and optimized most stable structures of Al-doped h-BN nanosheets are shown in Fig. 3. The doping impurity Al atom with larger size into

h-BN nanosheet induces the deformation of the six membered rings near the doping site of h-BN nanosheet to relieve stress, and results in the Al atom protruding out of the nanosheet (Fig. 3). The bond lengths for Al_B-N and Al_N-B bonds in Al-doped h-BN nanosheet were obtained 1.733 and 2.052 Å, respectively, are in agreement with previous report[20]. For Al-doped h-BN we also explore various possible adsorbing configurations of the mercaptans molecules and we find the most stable configuration is the structures as perpendicular with S atom of MeSH and EtSH pointing to Al in both of the Al_N and Al_B-doped h-BN nanosheets. In other configurations adsorption MeSH and EtSH on the Al-doped h-BN sheet was not observed. For the Al_B site adsorption, the bond lengths between the S and Al atom in the adsorbed configurations were calculated to be 2.460 and 2.456 Å for MeSH and EtSH, respectively, these values for the Al_N site adsorption were calculated to be 2.397 and 2.398 Å for MeSH and EtSH, respectively. This shows that adsorption of mercaptans on Al_N-doped h-BN nanosheet is a little stronger than adsorption of them on Al_B-doped h-BN nanosheet.

The calculated E_{ad} values for Al_N and Al_B-doped h-BN nanosheets are given in Table 1. The negative values of the E_{ad} indicate that adsorption is exothermic and thermodynamically favorable. These values also confirm stronger adsorption of the mercaptans molecules on Al_N-doped h-BN nanosheet in comparison with Al_B-doped h-BN nanosheet. The obtained E_{ad} values for adsorption of mercaptans molecules on Al-doped nanosheets is smaller than obtained values for B-vacancy defected h-BN nanosheet. The amount of charge transfer between mercaptans molecules and Al-doped h-BN nanosheet have also been reduced in comparison with B-vacancy defected h-BN nanosheet (Table 1). However, the values of E_{ad} and charge transfer reveals a chemical nature of adsorption on Al-doped h-BN nanosheet same as adsorption on B-vacancy defected h-BN nanosheet. We find the bond lengths of C-S in the adsorbed MeSH and EtSH on

the Al_B-doped h-BN nanosheet are about 1.826 and 1.841 Å, respectively, these values for Al_N site adsorption are 1.827 and 1.842 Å, respectively. These bond lengths are a little longer than that of the isolated MeSH (1.821 Å) and EtSH (1.828 Å) molecules, suggesting that the adsorption process weakens the S-C bond in compare of unadsorbed molecules.

One of the main purposes of developing sensors is to obtain sensors with lower recovery time. Therefore, recovery time plays a significant role in the preparation of the sensors. The recovery time, τ, according to the conventional transition state theory can be expressed as [24]:

$$\tau = \upsilon_0^{-1} \exp(\frac{-E_{ad}}{kT}) \qquad (3)$$

where T is temperature, k the Boltzmann's constant and v_0 the attempt frequency. As can be shown in the equation, increase the negative value E_{ad} will augment the recovery time in an exponential manner. Hence, to achieve reasonable recovery times the adsorption must not be strong. According to E_{ad} values obtained for MeSH and EtSH it can be concluded that the adsorption of the studied mercaptans molecules on Al-doped h-BN nanosheet are more favorable than adsorption on B-vacancy defected h-BN nanosheet.

Polarities are also obtained in the most stable geometries and are given in Table 1. The numerical values showed that the adsorption of mercaptans on Al_B-doped h-BN nanosheet cause an increase in the value of polarity in comparison with the polarity of the Al_B-doped h-BN nanosheet. In contrast the interaction of Al_N-doped h-BN nanosheet with studied mercaptans molecules cause a decrease in the value of the polarities.

The charge distribution can be explained by molecular electrostatic potential (MEP) calculation. MEP provides a valuable aid in the understanding of the sensor behavior. For instance, MEPs for MeSH, EtSH, Al_N-doped h-BN nanosheet, Al_N-doped h-BN/MeSH and Al_N-doped h-BN/EtSH nanosheet are shown in Fig. 4. As can be seen, the Al atom has a partial positive charge and the

S atom has a partial negative charge. Therefore, it can be concluded that these sites are reactive sites based Lewis acid-base reaction. This Fig. also shows a strong hybridization of the S and H atoms of studied mercaptans with Al atom of Al_N-doped h-BN nanosheet.

3.4. Frequency calculations

In order to verify the structures, corresponding frequency calculations were carried out at the same level. The results of the calculations did not produce any imaginary frequencies, confirming stability of the structures. The calculated Infrared (IR) spectra of the B-vacancy h-BN, B-vacancy h-BN/EtSH, Al_N-doped h-BN, and Al_N-doped h-BN/MeSH nanosheet structures are shown in Fig. 5 as model. The IR spectrum of B-vacancy h-BN nanosheet shows stronger IR bands correspond to those vibrational modes with frequencies of 875, 979, 992, 1468, 1492, 1503, 1513,1530 and 1555 cm^{-1}. While the IR bands at 875, 979 and 992 cm^{-1} are attributed to out-of-plane movement, the bands with frequencies of 1468, 1492, 1503, 1513, 1530 and 1555 cm^{-1} are associated with wagging of nanosheet. In the case of B-vacancy h-BN/EtSH nanosheet, there are some shifts in vibrational modes with respect to the B-vacancy h-BN nanosheet (890, 986, 1002, 1463, 1475, 1503, 1509, 1531, and 1545 cm^{-1}). The calculated IR spectrum of Al_N-doped h-BN nanosheet shows stronger bands with frequencies of 884, 980, 1004, 1262, 1341, 1375, 1425, 1439, 1470, 1496, 1512, 1532, and 1547 cm^{-1}. The IR bands at 884, 980 and 1005 cm^{-1} are related to out-of-plane movement and bands at 1262,1341,1375,1425,1439, 1470, 1496, 1512, 1532, and 1547 cm^{-1} are associated with wagging of nanosheet. In comparison with Al_N-doped h-BN nanosheet, Al_N-doped h-BN/MeSH nanosheet showed some shifts in vibrational modes. The IR spectrum of Al_N-doped h-BN/MeSH nanosheet shows stronger IR bands

frequencies at 884, 979, 1004, 1258, 1340, 1377, 1428, 1439, 1469, 1500, 1512, 1532, 1574 cm^{-1}.

3.5. Density of states (DOS)

To better understand the effect of having a defect, Al doping, and mercaptans adsorption for the electronic structure of h-BN nanosheet, the total electronic densities of states (DOS) for the pristine, defected, and Al-doped h-BN nanosheet with and without mercaptans adsorptions are plotted and displayed in Figs. 6 and 7 and Table 1. As can be seen, DOS analysis indicates the pristine h- BN nanosheet is a semiconductor with a wide HOMO-LUMO gap of 9.95 eV. Calculated DOS plots for defected h-BN nanosheet show a considerable change in E_g value from 9.95 eV in the pristine h-BN nanosheet to 6.59, 6.09, and 7.03 eV for B-vacancy, N-vacancy, and SW defected h-BN nanosheet, respectively, these decrease in E_g values due to defect are agreement with pervious report[21]. As can be seen in Fig. 6 and Table 1, for the adsorbed form of the MeSH and EtSH on the B-vacancy defected h-BN nanosheet in comparison that of the unadsorbed form, the E_g values a little changed from 6.59 to 6.63 and 6.39 eV, respectively.

The DOS of the Al-doped h-BN and mercaptans adsorbed on the Al-doped h-BN are shown in Fig. 7. As evident from Fig. 7, in comparison with pristine h-BN nanosheet, Al_B-doped h-BN nanosheet has a little decrease in E_g value and it is still a large-gap semiconductor and this is in good accordance with previous report[20]. But, Al_N-doped h-BN nanosheet has a considerable change of E_g value (see Table 1). The E_g value for Al_N-doped h-BN nanosheet decreased to 6.02 eV. It is well known that the electrical conductance of a material is related to its E_g value according to the following equation:

$$\sigma \alpha \exp(\frac{-E_g}{2kT}) \qquad (4)$$

where σ is the electrical conductivity and k is the Boltzmann's constant [29]. According to the equation, smaller values of E_g at a given temperature lead to larger electric conductivity. Therefore, electrical conductivity of the Al_N-doped h-BN in comparison with Al_B-doped h-BN and pristine h-BN nanosheet is enhanced and it seems that doping Al at N site of h-BN nanosheet is better than doping Al at B site. The calculated HOMO-LUMO gap of the MeSH and EtSH adsorbed onAl_B-doped h-BN are 9.40 and 9.37 eV, respectively. But these values for Al_N-doped h-BN nanosheets are 6.91 and 6.90 eV, respectively. Therefore, the DOS of Al_B-doped h-BN nanosheet did not show considerable changes due to MeSH and EtSH adsorption in the gap regions of the DOS plots, which indicates low sensitivity of the Al_B-doped h-BN. While in Al_N-doped h-BN nanosheet due to MeSH and EtSH adsorption considerable changes occurred in the gap regions of the DOS plots. It is revealed from DOS plots that their valence levels in both of the adsorbed configurations are approximately similar to that of the Al_N-doped h-BN nanosheet, while the conduction levels significantly have been shifted so that the E_g value of the Al_N-doped BNNT nanosheet is changed from 6.02 eV to 6.91 and 6.90 eV in adsorbed configurations (see Table 1). These show higher sensitivity of the Al_N-doped BNNT nanosheet toward studied mercaptans molecules in comparison with Al_B-doped BNNT nanosheet.

4. Conclusion

In this research, we have explored the adsorption of MeSH and EtSH molecules on the pristine, defected and Al-doped h-BN nanosheet by performing DFT calculations. The results indicate that pristine, N-vacancy, and SW defected h-BN nanosheet do not have sensitivity toward mercaptans molecules. In comparison, Al-doped and B-vacancy defected h-BN nanosheets showed high sensitivity for methyl and ethyl mercaptans and mercaptans prefer to be adsorbed

on these nanosheets through S atom. The adsorption energy values and Mulliken charge analyses showed the chemical nature of the interaction. The DOSs of pristine h-BN nanosheet are significantly changed due to creating defects, doping Al in N site and adsorbing mercaptans on B-vacancy defected and Al_N-doped h-BN nanosheets, whereas the DOSs of pristine h-BN nanosheet are slightly changed due to doping Al in B site and adsorbing mercaptans on Al_B-doped h-BN nanosheet.

References

1. A. S. Kudryavtsev, A. L. Makas, M. L. Troshkov, M. A. Grachev and S. P. Pod'yachev, *Talanta*, 2014, **123**, 140-145.
2. K.-C. Li and D. Shooter, *Int. J. Environ. Anal. Chem.*, 2004, **84**, 749-760.
3. C. Vassilakos, A. Papadopoulos, M. Lahaniati, T. Maggos, J. Bartzis and P. Papagianakopoulos, *Fresenius Environ. Bull.*, 2002, **11**, 516-521.
4. Y. Moliner-Martínez, R. Herráez-Hernández, C. Molins-Legua, J. Verdú-Andrés, M. Avella-Oliver and P. Campíns-Falcó, *Talanta*, 2013, **106**, 127-132.
5. S. Lousinian, N. Kalfagiannis and S. Logothetidis, *Solid State Sci.*, 2009, **11**, 1801-1805.
6. Z. Li and F. Gao, *Phys. Chem. Chem. Phys.*, 2012, **14**, 869-876.
7. N. Zhang, H. Liu, H. Kan, X. Wang, H. Long and Y. Zhou, *J. Alloys Compd.*, 2014, **613**, 74-79.
8. G. Kim, S. C. Jung and Y.-K. Han, *Curr. Appl. Phys.*, 2013, **13**, 2059-2063.
9. R. T. Paine and C. K. Narula, *Chem. Rev.*, 1990, **90**, 73-91.
10. C. Tang, Y. Bando, C. Liu, S. Fan, J. Zhang, X. Ding and D. Golberg, *J. Phys. Chem. B*, 2006, **110**, 10354-10357.
11. R. Ma, Y. Bando, H. Zhu, T. Sato, C. Xu and D. Wu, *J. Am. Chem. Soc.*, 2002, **124**, 7672-7673.
12. Z.-G. Chen, J. Zou, G. Liu, F. Li, Y. Wang, L. Wang, X.-L. Yuan, T. Sekiguchi, H.-M. Cheng and G. Q. Lu, *ACS Nano*, 2008, **2**, 2183-2191.
13. L. Xue, B. Lu, Z.-S. Wu, C. Ge, P. Wang, R. Zhang and X.-D. Zhang, *Chem. Eng. J.*, 2014, **243**, 494-499.
14. Y. Tian, X.-f. Pan, Y.-j. Liu and J.-x. Zhao, *Appl. Surf. Sci.*, 2014, **295**, 137-143.
15. J.-x. Zhao and Y.-h. Ding, *J. Chem. Phys.*, 2009, **131**, 014706.

16. R. Wang, D. Zhang and C. Liu, *Comp. Mater. Sci.*, 2014, **82**, 361-366.

17. J. Galicia Hernández, G. Cocoletzi and E. Anota, *J. Mol. Model.*, 2012, **18**, 137-144.

18. E. C. Anota, L. D. H. Rodríguez and G. H. Cocoletzi, *Graphene*, 2013, **1**, 124-130.

19. E. C. Anota, Y. Tlapale, M. S. Villanueva and J. A. R. Márquez, *J. Mol. Model.*, 2015, **21**, 1-6.

20. A. A. Peyghan, M. Noei and S. Yourdkhani, *Superlattices Microstruct.*, 2013, **59**, 115-122.

21. Y. Yamini and M. Moradi, *Sens. Actuators B Chem.*, 2014, **197**, 274-279.

22. S. Noorizadeh and E. Shakerzadeh, *Comp. Mater. Sci.*, 2012, **56**, 122-130.

23. J. Kaur, S. Singhal and N. Goel, *Superlattices Microstruct.*, 2014, **75**, 445-454.

24. J. Beheshtian, A. A. Peyghan and Z. Bagheri, *Sens. Actuators B Chem.*, 2012, **171–172**, 846-852.

25. M. W. Schmidt, K. K. Baldridge, J. A. Boatz, S. T. Elbert, M. S. Gordon, J. H. Jensen, S. Koseki, N. Matsunaga, K. A. Nguyen, S. Su, T. L. Windus, M. Dupuis and J. A. Montgomery, *J. Comput. Chem.*, 1993, **14**, 1347-1363.

26. J.-D. Chai and M. Head-Gordon, *Phys. Chem. Chem. Phys.*, 2008, **10**, 6615-6620.

27. N. M. O'Boyle, A. L. Tenderholt and K. M. Langner, *J. Comput. Chem.*, 2008, **29**, 839-845.

28. M. Castro and E. Chigo-Anota, *Mexican Journal of Materials Science and Engineering*, 2014, **1**, 21-29

29. S. S. Li, *Semiconductor physical electronics*, Springer Science & Business Media, 2007.

Legend of figures:

Fig. 1. Optimized configurations of (a) MeSH and EtSH, (b) pristine h-BN nanosheet, (c) SW defected h-BN nanosheet, and (d) N-vacancy defected h-BN nanosheet.

Fig. 2. Optimized configurations of (a) B-vacancy defected h-BN, (b) MeSH adsorbed on B-vacancy defected h-BN, (c) EtSH adsorbed on B-vacancy defected h-BN.

Fig. 3 . (a) Optimized configuration of Al_B-doped h-BN, (b) adsorbed configuration of MeSH on Al_B-doped h-BN, (c) adsorbed configuration of EtSH on Al_B-doped h-BN, (d) optimized configuration of Al_N-doped h-BN, (e) adsorbed configuration of MeSH on Al_N-doped h-BN, and (f) adsorbed configuration of EtSH on Al_N-doped h-BN.

Fig. 4. The MEPs of (a) MeSH, (b) EtSH, (c) Al_N-doped h-BN, (d) MeSH adsorbed on Al_N-doped h-BN, and (e) EtSH adsorbed on Al_N-doped h-BN. Color range: −0.04 to +0.04.

Fig. 5. IR spectra of (a) B-vacancy h-BN, (b) B-vacancy h-BN/EtSH, (c) Al_N-doped h-BN, and (d) Al_N-doped h-BN/MeSH nanosheet

Fig. 6. The DOSs of (a) pristine h-BN, (b) B-vacancy defected h-BN, (c) N-vacancy defected h-BN, (d) SW defected h-BN, (e) MeSH adsorbed on B-vacancy defected h-BN, and (f) EtSH adsorbed on B-vacancy defected h-BN. The Fermi level is set to zero.

Fig. 7. The DOSs of (a) Al_B-doped h-BN, (b) Al_N-doped h-BN, (c) MeSH adsorbed on Al_B-doped h-BN (d) EtSH adsorbed on Al_B-doped h-BN, (e) MeSH adsorbed on Al_N-doped h-BN, and (f) EtSH adsorbed on Al_N-doped h-BN. The Fermi level is set to zero.

Table 1

Calculated adsorption energy (E_{ad}), Dipolar moment (D), HOMO energies (E_{HOMO}), LUMO energies (E_{LUMO}), HOMO–LUMO energy gap (Eg), and net charge transfer Q_T.

System	E_{ad} (kcal mol^{-1})	D (Debye)	E_{LUMO} (eV)	E_{HOMO} (eV)	E_g (eV)	Q_T *(e)*
MeSH	-	1.7896	2.34	-8.71	11.05	-
EtSH	-	1.8796	2.34	-8.68	11.02	
pristine h-BN nanosheet	-	5.6904	1.40	-8.55	9.95	-
B-vacancy h-BN	-	5.4973	-2.01	-8.6	6.59	-
B-vacancy h-BN/MeSH	-43.10	6.8102	-1.27	-7.9	6.63	0.583
B-vacancy h-BN/EtSH	-44.78	6.9937	-0.28	-6.67	6.39	0.602
N-vacancy h-BN	-	5.4379	-0.06	-6.15	6.09	-
SW-defected H-BN	-	5.3534	0.98	-8.01	7.03	-
Al_B-doped h-BN	-	5.7314	1.02	-8.55	9.57	-
Al_B-doped h-BN/MeSH	-25.14	8.0456	1.03	-8.37	9.40	0.252
Al_B-doped h-BN/EtSH	-25.75	6.3208	1.04	-8.33	9.37	0.245
Al_N-doped h-BN	-	5.7833	-1.22	-7.24	6.02	-
Al_N-doped h-BN/MeSH	-30.65	5.7407	0.08	-6.83	6.91	0.267
Al_N-doped h-BN/EtSH	-31.46	5.5425	0.11	-6.79	6.90	0.262

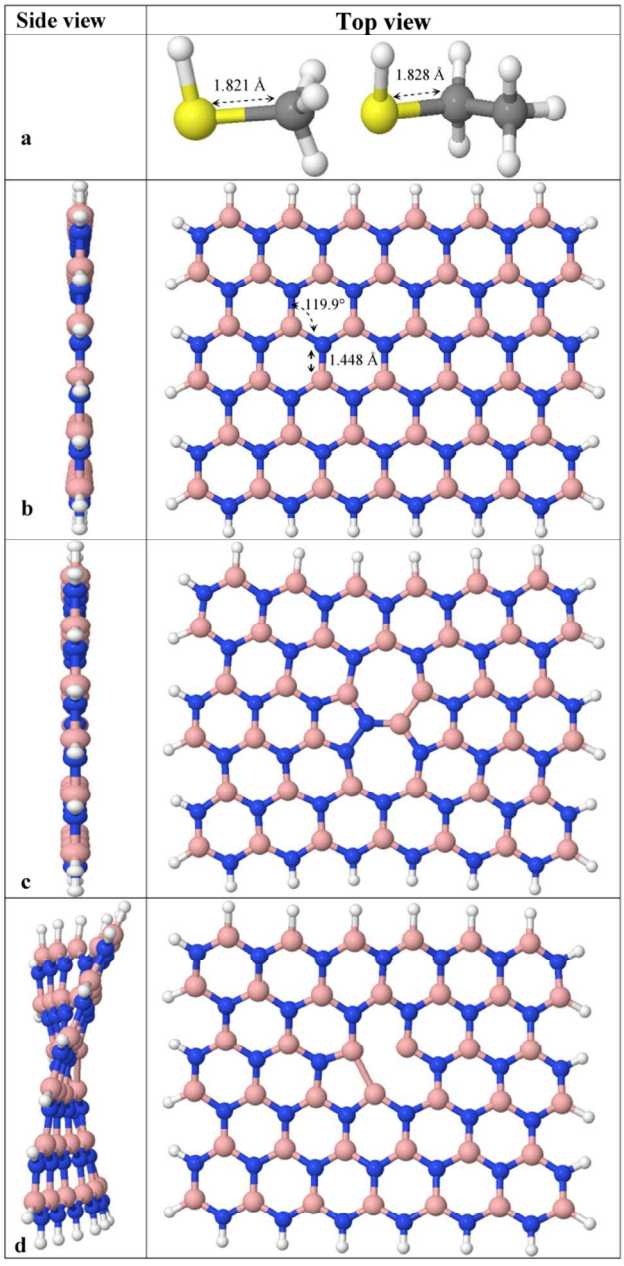

Fig. 1

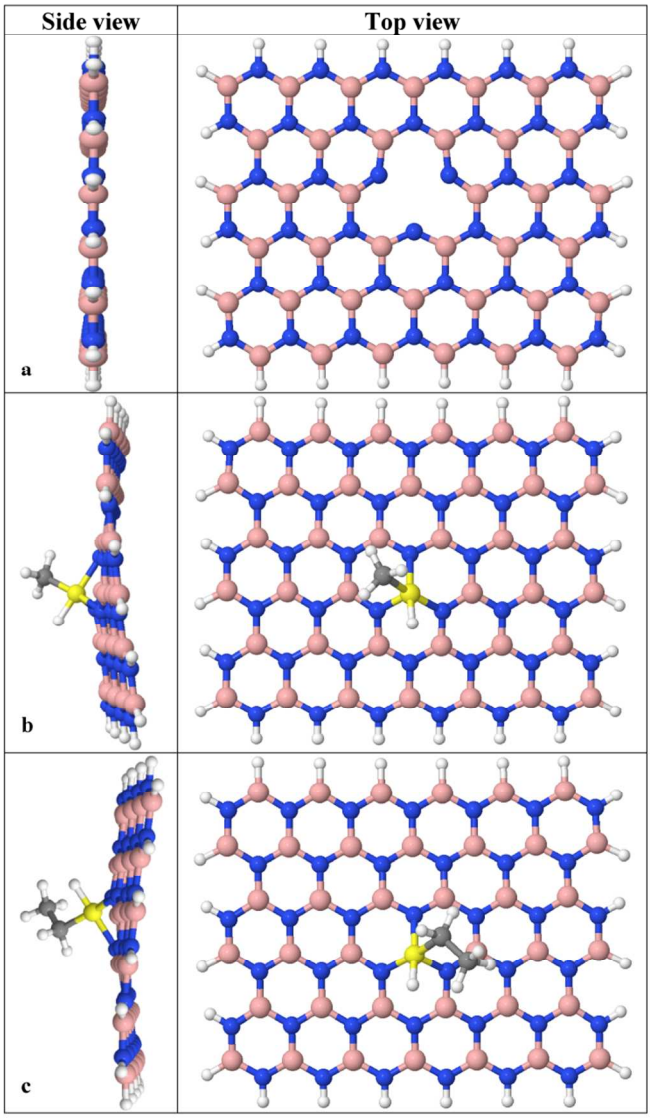

Fig. 2

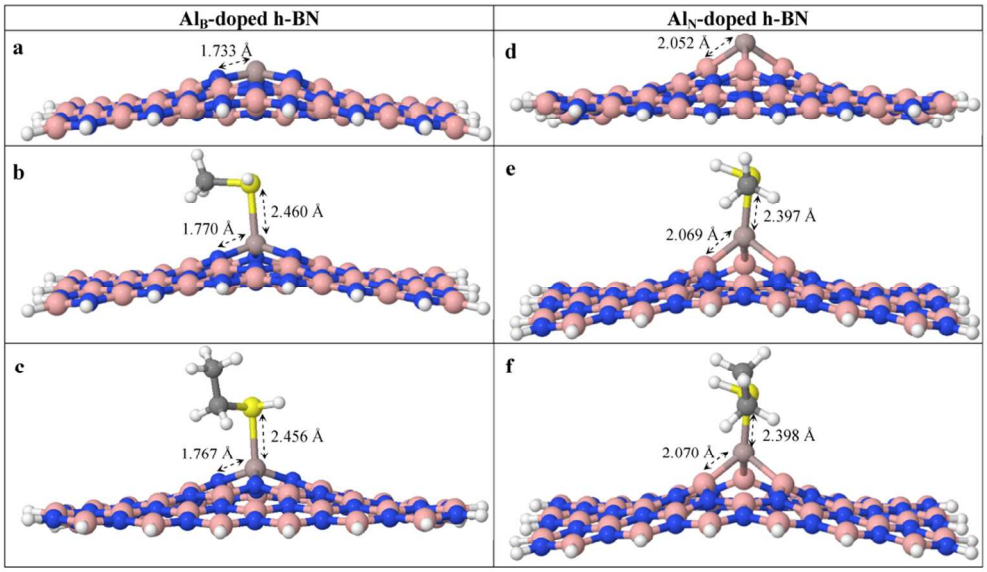
Al$_B$-doped h-BN
Al$_N$-doped h-BN
a
1.733 Å
d
2.052 Å
b
2.460 Å
1.770 Å
e
2.397 Å
2.069 Å
c
2.456 Å
1.767 Å
f
2.398 Å
2.070 Å

Fig. 3

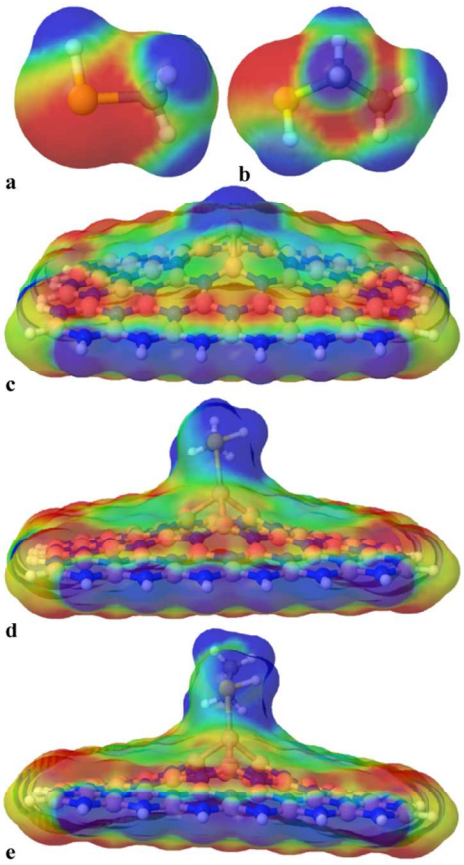

Fig. 4

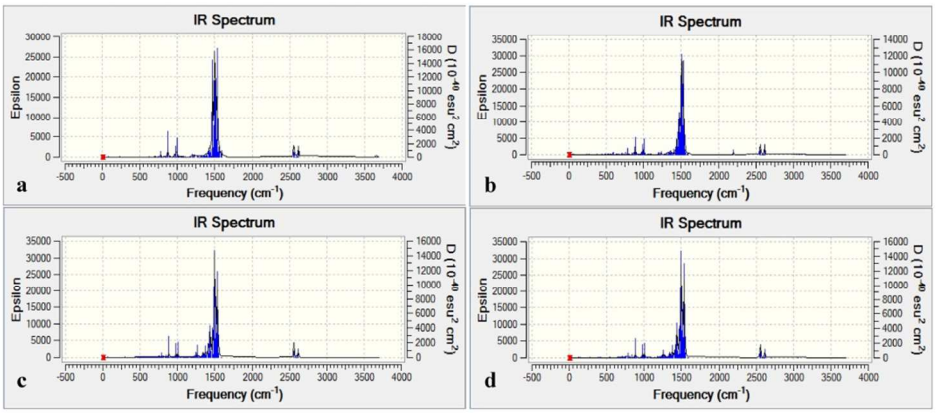

Fig. 5

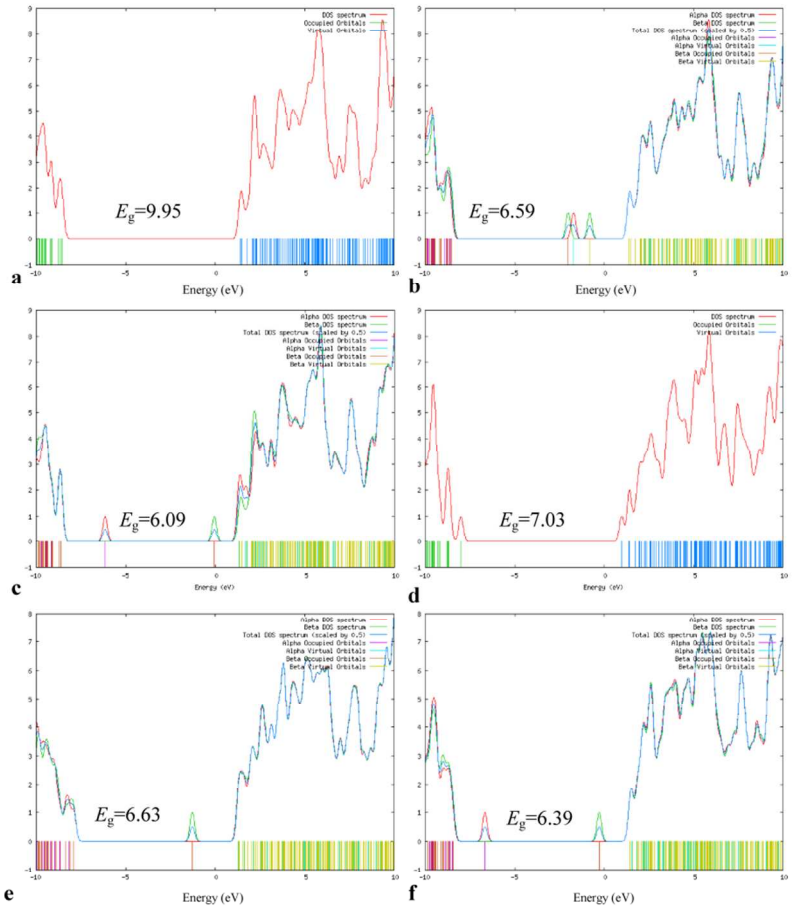
a
E_g=9.95
Energy (eV)
b
E_g=6.59
Energy (eV)
c
E_g=6.09
d
E_g=7.03
e
E_g=6.63
Energy (eV)
f
E_g=6.39
Energy (eV)

Fig. 6

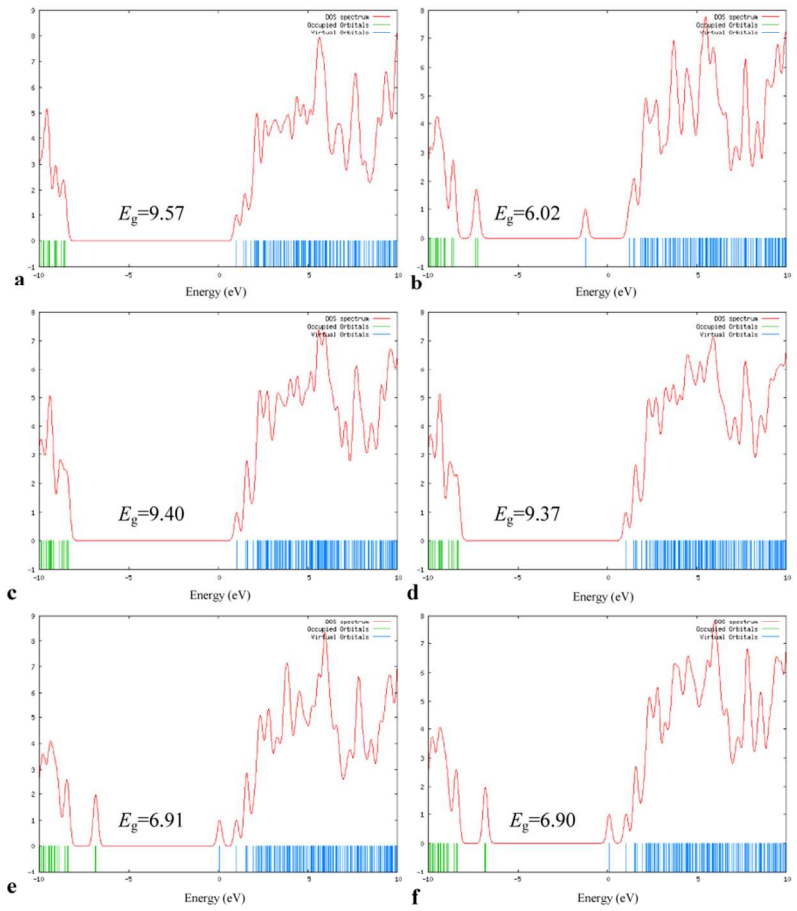
DOS spectrum
Occupied Orbitals
Virtual Orbitals
E_g=9.57
Energy (eV)
a
E_g=6.02
Energy (eV)
b
E_g=9.40
Energy (eV)
c
E_g=9.37
Energy (eV)
d
E_g=6.91
Energy (eV)
e
E_g=6.90
Energy (eV)
f

Fig. 7

We reported Al-doped hexagonal boron nitride nanosheet as a new adsorbent for mercaptans.

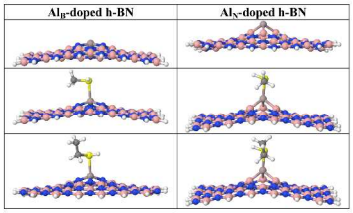

296x419mm (600 x 600 DPI)